NPL

NPL REPORT MAT 69

Hydrogen permeation modelling with generalised boundary conditions at the charging surface

A TURNBULL and L WRIGHT

August 2014

Hydrogen permeation modelling with generalised boundary conditions at the charging surface

Alan Turnbull and Louise Wright
Materials Division

SUMMARY

Diffusion and trapping of hydrogen in a low alloy steel has been modelled with the distinctive feature of generalised boundary conditions at the charging surface to replace the constant concentration or constant flux boundary conditions commonly adopted. Rates of hydrogen charging, chemical and electrochemical recombination of adsorbed hydrogen atoms, and absorption and desorption are incorporated. The adoption of such boundary conditions allows theoretical demonstration of the effect of specimen thickness on hydrogen permeation flux and sub-surface hydrogen concentration, and an assessment of the extent to which changing the charging current density can alter the balance between diffusion control and surface reaction control of hydrogen diffusion. As expected conceptually, a lower sub-surface hydrogen concentration is predicted for thin specimens compared with thick specimens and the suggestion that data from the former is more relevant to sulphide stress corrosion cracking is questioned. Partial surface reaction control of transport manifests itself in a reduced slope of the permeation flux-time curve relative to the prediction for thick specimens. For testing where the thickness of the specimen is limited, increasing the charging current density would be more likely to establish diffusion control transport.

The steady-state sub-surface hydrogen concentration is shown experimentally for steel to obey a square root dependence on charging current density but to attain a limiting value at higher current density. A theoretical explanation is proposed based on electrochemical recombination becoming the dominant recombination reaction as the applied current increases. There is some indication for controlled cathodic charging experiments that the effect on hydrogen uptake of poisons such as H_2S and arsenic may relate to their influence on the electrochemical recombination step rather than the chemical recombination step.

© Queens Printer and Controller of HMSO, 2014

ISSN 1754-2979

National Physical Laboratory
Hampton Road, Teddington, Middlesex, TW11 0LW

Extracts from this report may be reproduced provided the source is acknowledged and the extract is not taken out of context.

Approved on behalf of NPLML by Dr M Gee,
Knowledge Leader, Materials Team.

CONTENTS

1. INTRODUCTION

The electrochemical method for measuring hydrogen permeation in metals is the most common approach to determining hydrogen diffusivity and uptake, following from the initial novel work of Devanathan and Stachurski [1], and has since developed to international standardisation [2,3]. There have been many hundreds of measurements since, too numerous to record though see references [4-6]. Underpinning the extraction of data from these measurements is the adoption of models based on Fick's law [7] or the diffusion and trapping equations of McNabb and Foster [8] and Leblond and Dubois [9,10]. Fick's law becomes applicable only at low trap occupancy while the model of McNabb and Foster and of Leblond and Dubois, extended to include multiple traps is more widely relevant. Inherent in application of these models is the assumption that the experimental method is configured to satisfy the requirement of these models with respect to the boundary conditions. Most commonly this is based on controlling the charging conditions and adopting a sufficiently thick metal membrane such that the sub-surface concentration at the charging surface is constant, while at the oxidation surface the electrode potential is controlled to ensure the hydrogen concentration is effectively zero at that location. In the latter context the oxidation current is then a measure of the hydrogen flux.

While the standards give very specific guidelines to ensure that the testing methodology does satisfy the required boundary conditions (predominantly by increasing the thickness and ensuring the calculated diffusivity is independent of the thickness) there are too many occasions that these standards are ignored and the literature often populated with unreliable data. However, there are also applications when the material is available only as sheets of limited thickness and exploring the effect of thickness may not be an option. Then the question is how best to optimise the charging conditions to make it more likely that the parameters derived are close to the "intrinsic" value. There is also an argument in recent work by Kittel et al. [11] in relation to sulphide stress cracking that permeation data from thin carbon steel specimens that induce a constant flux boundary condition are most appropriate while for hydrogen induced cracking at internal voids it is diffusion controlled transport that is most relevant.

To address these different issues we have applied our hydrogen transport modelling incorporating generalised boundary conditions, first developed for 2-D modelling of hydrogen at a crack tip [12], to 1-D modelling of hydrogen transport through a membrane.

2. TRANSPORT EQUATIONS AND BOUNDARY CONDITIONS

2.1 Transport equations

The 3D form of the transport equations is shown in Appendix 1. Since the purpose of this work is to be illustrative it is sufficient to reduce the equations to a simpler form, assuming 1D diffusion appropriate to a metal membrane, only one type of reversible trap, neglect stress as this is not so relevant for most membrane tests, and assume the tortuosity factor is one. The equations then reduce to

$$\frac{\partial C}{\partial t} = D_L \frac{\partial^2 C}{\partial x^2} - \frac{\partial C_l}{\partial t} \tag{1}$$

$$\frac{\partial C_l}{\partial t} = N_r \left[k_r C_L (1-\theta_r) - p_r \theta_r \right] \tag{2}$$

which is the original form of the McNabb and Foster equations [8], where C is the concentration of hydrogen in lattice sites, C_l is the concentration of hydrogen in trap sites, N_r is the number of trap sites, θ_r is the trap occupancy, k_r and p_r are respectively the rate constants for jumping in and out of traps, and D_L is the lattice diffusion coefficient.

2.2 Initial and boundary conditions

The physical nature of the reactions at the metal solution interface is illustrated schematically in Figure 1.

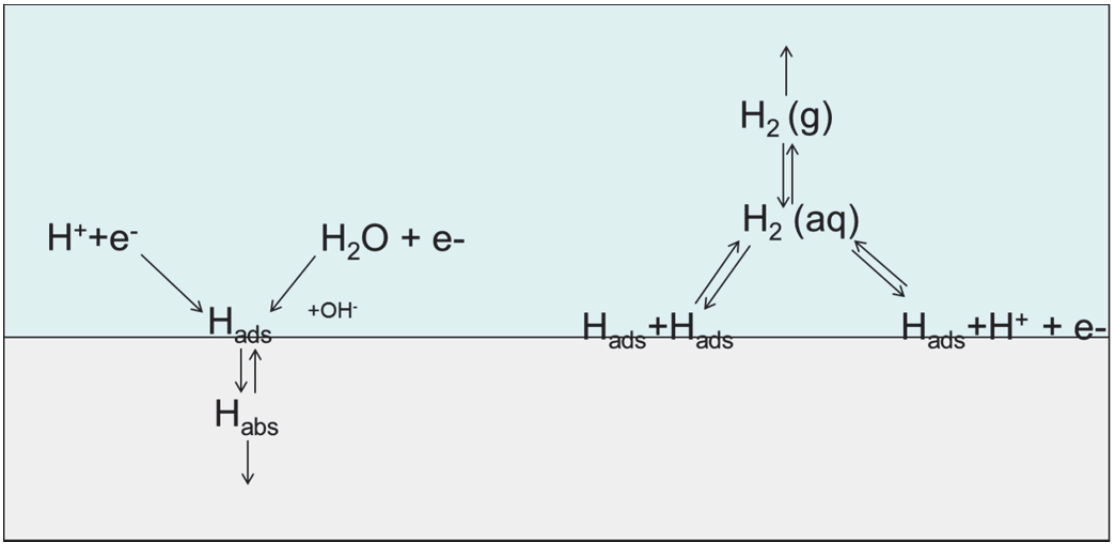

Figure 1: Schematic illustration of reaction processes at charging surface.

The predominant cathodic reduction reaction involves both reduction of protons and water with the relative magnitude dependent on the local pH in the solution at the metal surface. The evolution of hydrogen also involves two processes, chemical recombination (Tafel reaction) of adsorbed hydrogen atoms and electrochemical recombination (Heyrovsky reaction) involving both the adsorbed hydrogen and the proton (though H_2O could perhaps be directly involved in the hydrogen evolution process at high pH, rather than hydrogen ions). Recent work [13] has demonstrated that direct cathodic reduction of H_2S can occur and this has to be considered as an additional process in sour environments for both electrochemical charging and electrochemical recombination.

The initial and boundary conditions are:

at t=0, all x: C=0

For t>0, x=0 (oxidation surface) C=0

For t>0, x=L (charging surface):

$$J_{in} = D_L \frac{\partial C}{\partial x} = \left\{ \frac{i_c}{F} - \frac{i_r^{chem}}{F} - \frac{i_r^{elect}}{F} \right\} \quad (3)$$

$$= \left\{ k_1 \theta_{ad} - k_{-1} C_0 (1 - \theta_{ad}) \right\} \quad (4)$$

with

the charging current density given by: $i_c = k_c(1 - \theta_{ad})$

the chemical recombination rate by: $i_r^{chem} = k_r^{chem}\theta_{ad}^2$

the electrochemical recombination current density by: $i_r^{elect} = k_r^{elect}\theta_{ad}$

and the absorption and desorption rate constants by k_1 and k_{-1} respectively. C_0 is the sub-surface hydrogen concentration, F is Faraday's constant.

3. PARAMETERS

Deriving all the relevant parameters for the boundary conditions is a challenge. For this analysis use was made of measurements undertaken previously for an AISI 4340 steel [12] in which the methodology proposed by Iyer et al. [14] was used to determine the chemical recombination rate constant. There is no specific information on the electrochemical recombination current density; the derivation for this analysis is described in Appendix 2. The key assumption adopted was that the transfer coefficient would be identical to that for the cathodic reduction current density so that distinction in magnitude of the two current densities would reside only in the pre-exponential factor.

As noted previously [12], the absorption and desorption rate constants are not readily accessible, though the equilibrium constant can be determined from permeation experiments [14]. Accordingly, the assumption was made that these rate constants are very large compared to other reaction rate constants, and also the diffusion flux, so that equilibrium between adsorbed and absorbed hydrogen atoms is always maintained.

The relevant parameters adopted for the analysis are listed in Table 1.

Table 1: List of parameters. The use of ppm (parts per million by mass with 1 ppm = 4.76×10^{18} atoms/cm^3 and sites notionally equivalent to atoms) was a convenient normalisation to avoid extremes of numbers. See also reference [12] for the source of some data.

Parameter	Value	Units	Value	Units
N_1	2.2×10^{18}	sites/cm^3	0.46	ppm
k_1	3.4×10^{-17}	cm^3/s/trap site	161.8	(ppm s)$^{-1}$
p_1	0.031	s^{-1}	0.031	s^{-1}
D_L	7.2×10^{-5}	cm^2/s	7.2×10^{-5}	cm^2 s^{-1}
k_1	1.0×10^{7}	mol/cm^2/s	1.26×10^{12}	ppm cm s^{-1}
k_{-1}	8.8×10^{11}	cm/s	8.8×10^{11}	cm/s
$k_w (i_c/F)$	5.0×10^{-10}	mol/cm^2/s	6.32×10^{-5}	ppm cm s^{-1}
$k^*_w (k_r^{chem}/F)$	2.2×10^{-3}	mol/cm^2/s	2.78×10^{2}	ppm cm s^{-1}
$k'_w/(k_r^{elect}/F)$	5.0×10^{-7}	mol/cm^2/s	6.32×10^{-2}	ppm cm s^{-1}
N_L	5.2×10^{23}	sites/cm^3	1.09×10^{5}	ppm

The effect of varying the charging current density was also explored.

4. RESULTS AND DISCUSSION

4.1 Effect of specimen thickness

The initial interest in this study was to examine the effect of specimen thickness on the sub-surface hydrogen concentration at the input surface. The time-evolution of that value for different thickness of specimen is shown in Figure 2. The diffusion flux at the charging surface is shown in Figure 3. Calculations were extended to very thin specimens, much thinner than would be used in most testing, in order to demonstrate the trend as the model will tend to

underestimate the thickness required to ensure diffusion control (e.g. lack of consideration of surface film on oxidation surface).

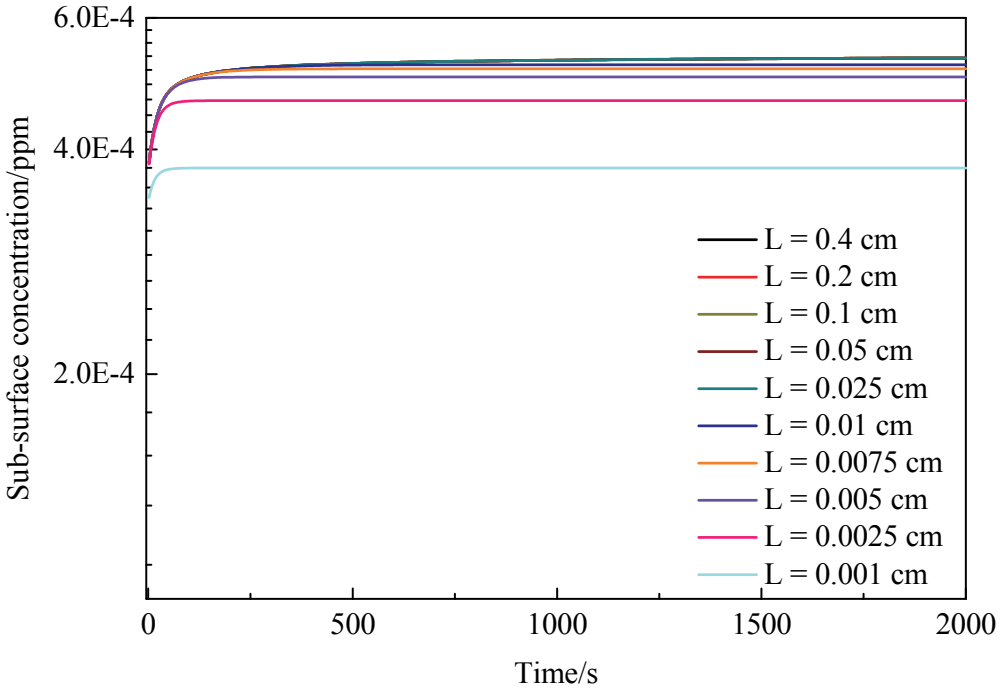

Figure 2: Calculated variation of the sub-surface concentration of hydrogen atoms as a function of time and specimen thickness; charging current density of 48 μA/cm^2.

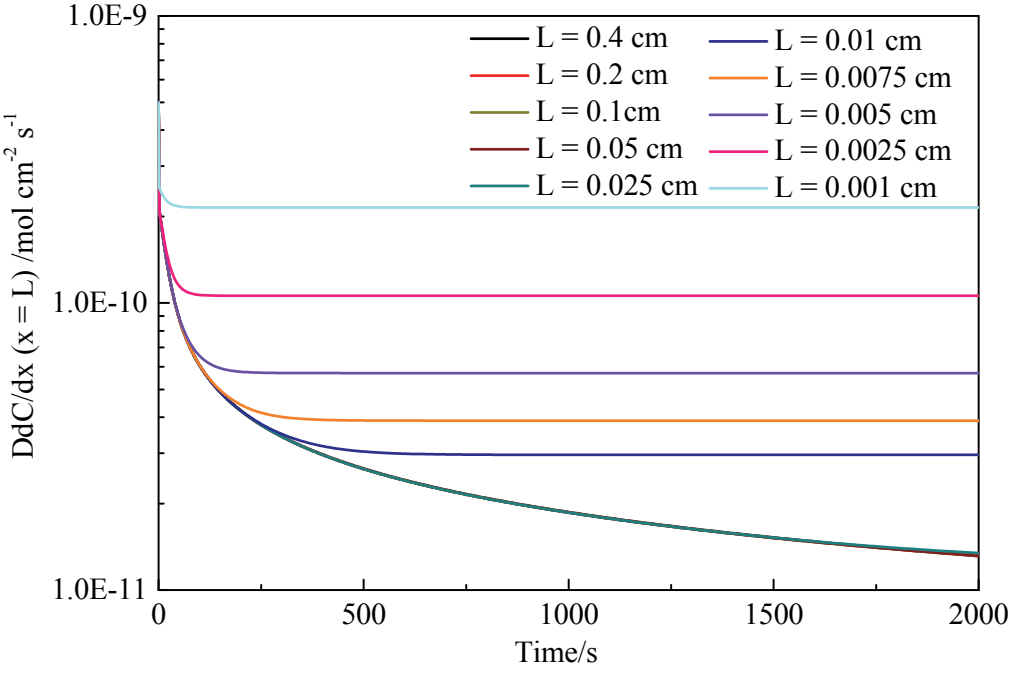

Figure 3: Calculated flux at charging surface as a function of thickness and time for charging current density of 48 μA/cm^2.

As the specimen thickness increases there is convergence of data such that the curves overlap and cannot be distinguished in these figures. As expected, there is a time delay in establishing a steady concentration and that is more pronounced for the thicker specimen reflecting the time to achieve diffusion control of hydrogen transport in the latter case. In essence, the diffusion flux at short times (Figure 3) is relatively large as the concentration gradient is initially large and significant compared with the recombination reaction rate.

For very thin specimens diffusion control is not achieved at any stage and the steady-state value of C_0 is reduced compared with that for thick specimens. Under diffusion control conditions the flux would be small compared to the charging and recombination fluxes so that C_0 would be determined by the relative rates of the charging and recombination fluxes, which would almost be equal. As the specimen gets progressively thinner the diffusion flux should tend towards the value of the charging flux, as is observed. There would also be an experimental challenge in ensuring that oxidation of hydrogen was sufficiently rapid compared to the recombination reaction at the oxidation surface.

The suggestion by Kittel et al. [11] that hydrogen permeation data from thin specimen is most relevant for sulphide stress cracking would lead to non-conservative results as the C_0 values would be somewhat smaller than for a thicker specimen, albeit the difference is predicted to be quite small in the context of experimental variability. It would be seem to be misplaced logic by Kittel et al. since test times in sulphide stress corrosion cracking would be long compared to establishing the "steady" value of C_0. In reality, the corrosion rate in sulphide environments would be changing with time because of film formation so C_0 would evolve with time for other reasons but this does not negate the principle that thicker specimens will tend to lead to locally higher concentrations of hydrogen at the reacting surface.

The effect of specimen thickness on the predicted permeation current density as measured at the oxidation surface can be best expressed by plotting the normalised flux vs a normalised time, τ , where $\tau=D_L t/L^2$, as shown in Figure 4. The slope of the curves converges with increasing thickness, suggesting diffusion control. For thin specimens the slope is relatively shallow and this correlates with experimental observation [15] that a slope shallower than Fick's law on a dimensionless plot such as this is often an indication of surface reaction control, though a slope steeper than Fick's law does not necessarily imply diffusion control.

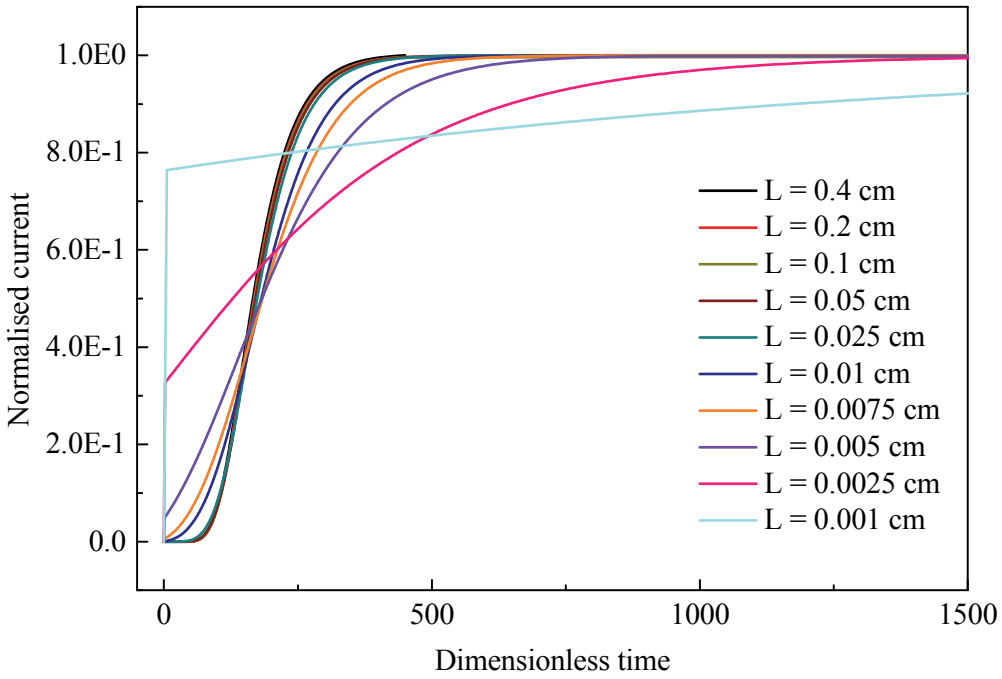

Figure 4: Normalised permeation current density at oxidation surface as a function of dimensionless time and thickness for charging current density of 48 $\mu A/cm^2$.

There can be situations in which there is no opportunity to increase the thickness of specimen because of limitations in the source, thin low alloy steel sheet for motor vehicle applications for example. The only variable that can be controlled is the charging current density. The question then is whether increasing or decreasing the charging current density would make it more or less likely that diffusion control would be achieved. Accordingly, computations were undertaken to evaluate the effect of charging current density on the permeation flux (Figure 5). The thickness chosen was 0.0075 cm as the normalised flux at this value was clearly deviating from the convergent value for the thicker specimens but not by a large amount. Since the steepness of the permeation transient would increase simply due to increased trap occupancy similar computations were undertaken for the 0.4 cm thick specimen as reference. It is evident that the best option to take when specimen thickness is limited is to increase the charging current density as the permeation flux will be closer to that diffusion control condition and the effective value of the diffusion coefficient will have less error. A possible limitation is excessive formation of hydrogen gas bubbles on the surface and vigorous stirring of the charging solution is advised.

In concluding this section it should be emphasised that the main goal was to highlight trends in the permeation behaviour in response to thickness and charging conditions. The data should not be used directly to set a minimum thickness for experimental testing as that will be system dependent.

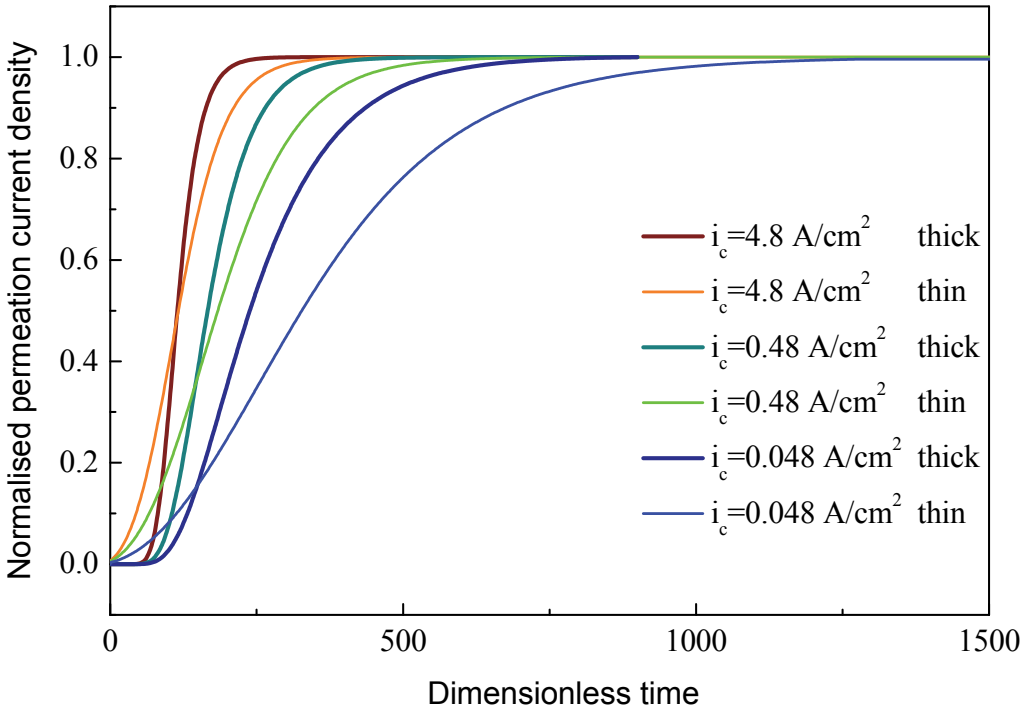

Figure 5: Effect of charging current density on normalised permeation flux vs dimensionless time for a thick specimen (0.4 cm) and for a relatively thin specimen (0.0075 cm).

4.2 Significance of electrochemical recombination

Experimental measurement, and conceptual thinking, suggests that with increase in the charging current density a limiting surface coverage and sub-surface concentration of hydrogen should be achieved. In essence, any further increase in the charging current should increase the electrochemical recombination current proportionally. An experimental example of this behaviour from permeation studies on a duplex stainless steel under cathodic charging is shown in Figure 6 [16]. Here, with no H_2S, a limiting sub-surface concentration of hydrogen is

obtained. In this particular plot the total hydrogen, lattice and reversibly trapped hydrogen, is plotted but at steady state the C_0 value will scale as the C_{0R} value. The square root dependence of the sub-surface hydrogen concentration reflects the balance between charging and chemical recombination while the limiting value in H_2S-free solution was considered to reflect the impact of electrochemical recombination.

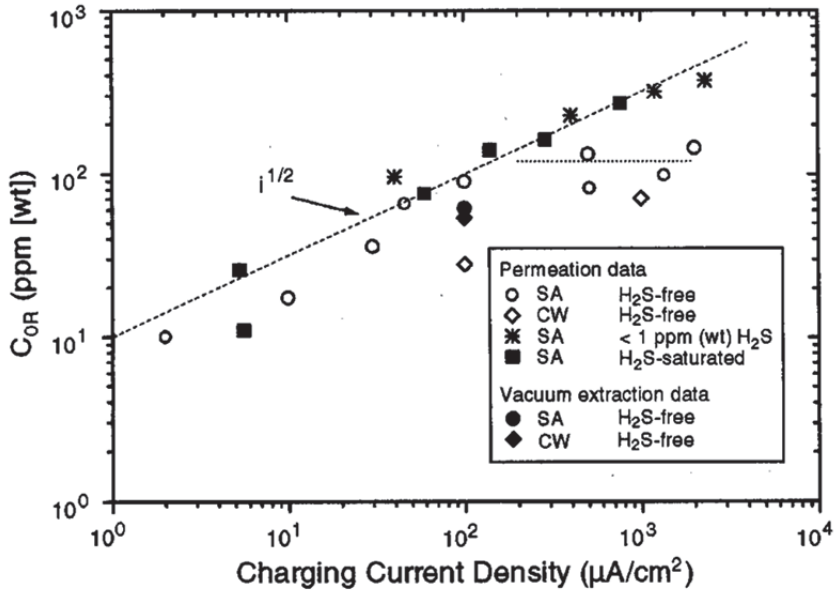

Figure 6: Experimental determined values of the total sub-surface concentration of lattice and reversibly trapped hydrogen atoms at steady state for duplex stainless steel in simulated oilfield environments at 80 ºC [16].

Computations to validate this concept are shown in Figure 7 for two values of the electrochemical recombination current density, while an analytical solution at steady state is included in Appendix 3. The figure replicates the trend well, square root dependence then a limiting C_0, with the onset of the limiting value shifted to higher current densities when the electrochemical reaction rate constant is reduced. Direct quantitative comparison with Figure 6 is not meaningful as the parametric database is for a different steel. Decreasing the chemical recombination rate constant has the expected effect of increasing the sub-surface hydrogen concentration because the rate of removal of adsorbed hydrogen decreases relative to the rate of generation from charging.

An interesting feature of Figure 6 is the lack of effect of H_2S on the chemical recombination behaviour, despite its well-established efficacy as a recombination poison [17]. However, it does appear to reduce the efficiency of the electrochemical recombination reaction to the extent that the tendency to a limiting C_0 is delayed to a much higher current density than was investigated. It seems unlikely that this involves direct reduction of the H_2S per se as that might be expected to be different for saturated H_2S and 1 ppm H_2S, suggesting that there is some effect of H_2S on the M-H bond. A similar behaviour to that of Figure 6 has been reported by Robinson et al [18] for an iron base superalloy in sulphuric acid with arsenic, though the data were perhaps less well-defined. Notably, there was no effect of the poison until higher charging current densities and a tendency for a limiting current in the absence of poison. However, the latter was attributed to formation of hydrogen bubbles with no discussion of electrochemical recombination.

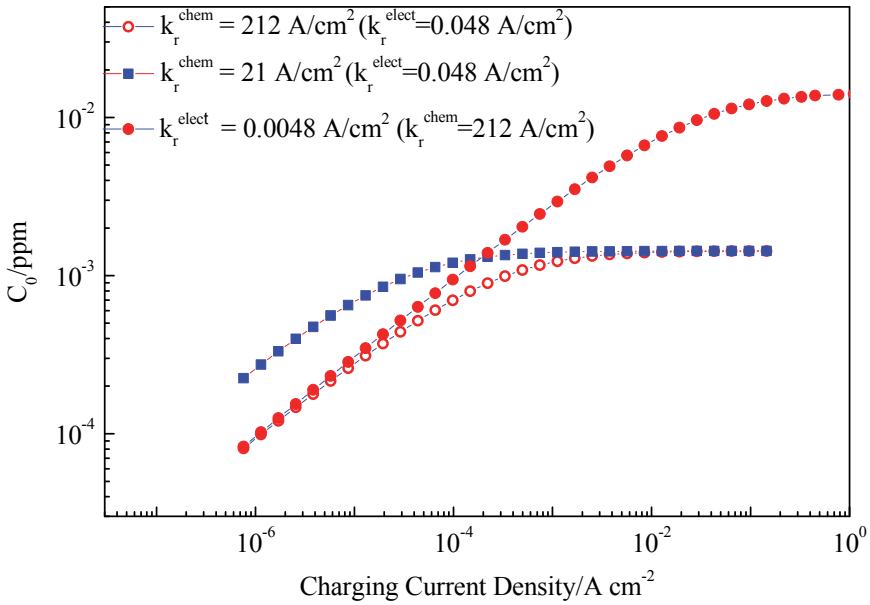

Figure 7: The sub-surface lattice concentration of hydrogen as a function of charging current density demonstrating the limiting value as electrochemical recombination becomes dominant and the decrease in magnitude with increase in chemical recombination rate constant.

5. CONCLUSIONS

The use of generalised boundary conditions for hydrogen permeation through a membrane highlights the importance of having a sufficiently thick specimen as prescribed in relevant standards.

A plot of permeation flux vs normalised time shows a reduced slope when the thickness becomes small. Experimental observation of such a reduced slope compared to Fick's law is the first indication that diffusion control has not been achieved. However, the converse is not necessarily true.

A modest reduction in the sub-surface concentration is predicted as the specimen becomes progressively thinner. This is not an unexpected observation but implies that the suggestion of Kittel et al. of adopting thin specimens as being most relevant for sulphide stress corrosion cracking tests would lead to non-conservative behaviour, though the effect would probably not be discernible experimentally.

Where the ideal thickness of specimen is not achievable, because the material is only manufactured in thin sheets, and diffusion is relatively fast testing with a high charging current density will tend to minimise the error in determining the effective diffusion coefficient. However, stirring of the solution to limit accumulation of gas bubbles on the surface is advised.

Inclusion of the electrochemical recombination current density along with chemical recombination leads to prediction of a limiting current density with increase in charging current density, as measured experimentally and conceptually predicted. Comparison with experiment suggests that poisons reduce the efficiency of the electrochemical recombination step.

6. REFERENCES

1. M.A.V. Devanathan and Z. Stachurski, Proc. Roy. Soc., A270 (1962) 90-101.
2. ASTM G148-9. 'Standard Practice for Evaluation of Hydrogen Uptake, Permeation, and Transport in Metals by an Electrochemical Technique', ASTM International. Philadelphia.
3. ISO 17081. 'Method of measurement of hydrogen permeation and the determination of hydrogen uptake and transport in metals by an electrochemical technique', ISO, Geneva.
4. A. Turnbull (ed.), Hydrogen transport and cracking in metals, Institute of Materials, London, 1995.
5. A. Turnbull, 'Hydrogen diffusion and trapping in metals', in Gaseous Hydrogen Embrittlement of High Performance Metals in Aqueous Systems, eds. R.P. Gangloff and B.P. Somerday, Woodhead Publishing, 2012, pp 89-124.
6. T. Boellinghaus, H. Hofmeister and A. Dangeleit, Welding in the World, 35 (1995) 83-96.
7. J. Crank, The Mathematics of Diffusion, 2nd edition, Clarendon Press, Oxford, 1975.
8. A. McNabb and P.K. Foster, Trans Metall. Soc., AIME, 227 (1963) 618-627.
9. J.B. Leblond and D. Dubois, Acta Metall., 31 (1983) 1459-1469.
10. J.B. Leblond and D. Dubois, Acta Metall., 31 (1983) 1471-1478.
11. J. Kittel, F. Ropital and J. Pellier, Corrosion, 64 (2008) 788-799.
12. A. Turnbull, D.H. Ferriss and H. Anzai, Mat. Sci. Eng., A206 (1996) 1-13.
13. J. Kittel, F. Ropital, F. Grosjean, E. M. M. Sutter, B. Tribollet, Corros. Sci., 66 (2013) 324-329.
14. R.B. Hutchings and A. Turnbull, 'Effect of charging environment on hydrogen permeation in low alloy steels', in Eurocorr '92, Barcelona, 1992.
15. R.N. Iyer, H.W. Pickering and M. Zamanzadeh, Scripta Metall., 22 (1988) 91-916.
16. A.J.Griffiths and A. Turnbull, Corrosion, 57 (2001) 165-174.
17. E. Protopopoff and P. Marcus, 'Surface effects on hydrogen entry into metals', in Corrosion Mechanisms in Theory and Practice, ed. P. Marcus, Marcel-Dekker, New York-Basle, 2002, 53-96.
18. S.L. Robinson, N.R. Moody, S.M. Myers, J.C. Farmer and F.A. Greulich, J. Electrochem. Soc., 137 (1990) 1391-1397.

7. APPENDIX 1: 3D FORM OF TRANSPORT AND BOUNDARY CONDITIONS

Transport equations:

$$\frac{\partial \mathrm{C}}{\partial \mathrm{t}} = \omega \mathrm{D}_L \nabla^2 \mathrm{C} + \nabla\left(- \frac{\omega \mathrm{D}_L \mathrm{C}}{R\,\mathrm{T}} . \mathrm{V}_\mathrm{H} \nabla \sigma_h \right) - \frac{\partial \mathrm{C}_1}{\partial \mathrm{t}} - \frac{\partial \mathrm{C}_2}{\partial \mathrm{t}} \tag{A1}$$

$$\frac{\partial \mathrm{C}_1}{\partial \mathrm{t}} = \mathrm{N}_1 \left[k_1 C_L (1-\theta_1) - p_1 \theta_1 \right] \tag{A2}$$

$$\frac{\partial \mathrm{C}_2}{\partial \mathrm{t}} = \mathrm{N}_2 \left[k_2 C_L (1-\theta_2) - p_2 \theta_2 \right] \tag{A3}$$

where ω is the tortuosity factor, $\mathrm{V_H}$ is the partial molar volume of the hydrogen atom, R is the gas constant, T is the temperature and two type of traps are considered.

The generalised boundary condition at the charging surface at t >0 (with boundary conditions as defined in main text) is now

$$J_{in} = D_L \frac{\partial C}{\partial n} - \frac{DV_H}{RT} C \frac{\partial \sigma_h}{\partial n} = \left\{ \frac{i_c}{F} - \frac{i_r^{chem}}{F} - \frac{i_r^{elect}}{F} \right\} \quad \text{(A4)}$$

$$= \left\{ k_{abs} \left[\exp\left(\frac{V_H}{RT} \sigma_h \right) \right] \theta_{ad} - k_{des} C_s (1 - \theta_{ad}) \right\} \quad \text{(A5)}$$

8. APPENDIX 2: DERIVATION OF ELECTROCHEMICAL RECOMBINATION RATE CONSTANT

There are three primary reactions occurring at the charging surface:

Cathodic reduction: $\frac{\mathrm{i_c}}{\mathrm{F}} = \frac{k}{F} \exp[-\gamma E_p](1-\theta) = k_w(1-\theta)$

Chemical recombination: $\frac{i_r^{chem}}{F} = k_w^* \theta^2$

Electrochemical recombination: $\frac{i_r^{elect}}{F} = \frac{k'}{F} \theta \exp[-\gamma' Ep] = k_w' \theta$ (assumes well buffered system)

Where Ep is the electrode potential.

Thus,

J $= k_w(1-\theta) - k_w^* \theta^2 - k_w' \theta$

Parameters:

γ=19.81
γ'=19.81 (assumed)

By implication the charging and recombination current densities will scale proportionally so that the value for only one charging current density is required. There is no a priori way to determine the pre-exponential factor except by experimental measurement or by experimental fit from these predictions, which will be feasible when more data become available. Unfortunately, the data for the present calculations is based on measurements on AISI 4340 steel but the experimental data of Figure 6 are for a duplex stainless steel. Hence, the choice of rate constant is of necessity arbitrary. We assume a value that is 1000 time less than that for the charging current density as a starting point.

9. APPENDIX 3: ANALYTICAL SOLUTION FOR C_0 VS CHARGING CURRENT DENSITY AT STEADY STATE

General form of boundary condition:

$$J_w = D\mathbf{n}.\nabla C - \frac{DV_H}{RT} C\mathbf{n}.\nabla \sigma_m = k_1 \theta_w \exp\left(\frac{V_H \sigma_m}{RT}\right) - k_{-1} C(1-\theta_w)$$
$$= k_w(1-\theta_w) - k_w^* \theta_w^2 - k_w' \theta_w$$

Form for a 1-D model applied on $x = L$ with zero stress:

$$J_w = D\frac{\partial C}{\partial x}\Big|_{x=L} = k_1\theta_w - k_{-1}C(1-\theta_w) = k_w(1-\theta_w) - k_w^*\theta_w^2 - k_w'\theta_w$$

Overall governing equation and boundary and initial conditions, assuming 1-D and one type of trap:

$$\frac{\partial C}{\partial t} = D\frac{\partial^2 C}{\partial x^2} - N_r\frac{d\theta_r}{dt}$$

$$\frac{d\theta_r}{dt} = k_r C(1-\theta_r) - p_r\theta_r$$

$$C(0,t) = 0$$

$$D\frac{\partial C}{\partial x}\Big|_{x=L} = k_1\theta_w - k_{-1}C(1-\theta_w) = k_w(1-\theta_w) - k_w^*\theta_w^2 - k_w'\theta_w$$

$$C(x,0) = 0$$
$$\theta_r(x,0) = 0$$

Consider the steady state

$$D\frac{\partial^2 C}{\partial x^2} = 0$$

$$k_r C(1-\theta_r) - p_r\theta_r = 0$$

so that, applying the boundary condition at $x = 0$,

$$C = Ax$$

$$\theta_r = \frac{k_r Ax}{(p_r + k_r Ax)}$$

and A is determined by the flux boundary condition:

$$DA = k_1\theta_w - k_{-1}AL(1-\theta_w) = k_w(1-\theta_w) - k_w^*\theta_w^2 - k_w'\theta_w$$

where AL is the concentration on the surface.

Rearranging the first equality to give θ_w in terms of A

$$\theta_w = \frac{(k_{-1}L + D)A}{(k_1 + k_{-1}AL)}$$

or, for A in terms of θ_w,

$$A = \frac{k_1\theta_w}{(k_{-1}L(1-\theta_w) + D)}$$

The second equality can be rearranged to give

$$k_w^*\theta_w^2 + (k_1 + k_w' + k_w + k_{-1}AL)\theta_w - k_{-1}AL - k_w = 0$$

Substituting in for θw:

$$k_w^*\left(\frac{(k_{-1}L + D)A}{(k_1 + k_{-1}AL)}\right)^2 + (k_1 + k_w' + k_w + k_{-1}AL)\frac{(k_{-1}L + D)A}{(k_1 + k_{-1}AL)} - k_{-1}AL - k_w = 0$$

or

$$k_w^*\big((k_{-1}L + D)A\big)^2 + (k_1 + k_w' + k_w + k_{-1}AL)(k_1 + k_{-1}AL)(k_{-1}L + D)A - (k_{-1}AL + k_w)(k_1 + k_{-1}AL)^2 = 0$$

which is cubic in A. Expanding and collecting terms gives:

$$D[k_{-1}]^2L^2A^3 + [([k_{-1}]^2L^2[k_w' + k_w^*] + Dk_{-1}L[2k_1 + k_w' + k_w + 2k_w^*] + D^2k_w^*)]A^2 + k_1\big[k_{-1}L[k_w' - k_w] + D[k_1 + k_w' + k_w]\big]A - k_w[k_1]^2 = 0$$

This expression is not easy to interpret in terms of a relationship between surface concentration and k_w or k_w', and an analytical solution (whilst available) is complicated to express and unlikely to be any clearer.

Suppose that we have a system with the following values:

Parameter	Value	Units	Value	Units
D	7.2×10^{-5}	cm^2/s		
k_1	1.0×10^{7}	$mol/cm^2/s$	$1.26\times x10^{12}$	ppm cm s^{-1}
k_{-1}	8.8×10^{7}	cm/s	8.8×10^{11}	cm/s
k_w*	2.2×10^{-3}	$mol/cm^2/s$	2.78×10^{2}	ppm cm s^{-1}
L	0.1	cm		

and that we assume that k_w and k_w' vary such that their ratio is a constant, and that all other values are held constant.

The coefficient of the cubic term is typically at least an order of magnitude smaller than the other coefficients. The coefficient of the quadratic term is dominated by the expression

$$[k_{-1}]^2L^2[k_w' + k_w^*]$$

and this term is well approximated by

$$[k_{-1}]^2L^2k_w^*$$

for most values of k_w' examined.

In the linear term, k_w' dominates k_w since it is 1000 times larger, and k_1 dominates both so that the linear term is well approximated by

$$k_1[k_{-1}Lk_w' + Dk_1]$$

Then we can approximate the equation by

$$[([k_{-1}]^2L^2k_w^*)]A^2 + k_1\big[k_{-1}Lk_w' + D[k_1]\big]A - k_w[k_1]^2 = 0$$

so that, after some rearrangement

$$A = \frac{C_{surf}}{L} = \frac{-k_1[k_{-1}Lk_w' + Dk_1] + k_1\sqrt{(k_{-1}Lk_w' + Dk_1)^2 + 4[k_{-1}]^2L^2[k_w^*]k_w}}{2([k_{-1}]^2L^2k_w^*)}$$

and this expression is a good approximation for all cases where the the terms listed above can be neglected.

For a small k_w', the second term under the square root dominates, and

$$\frac{C_{surf}}{L} = \frac{-k_1[k_{-1}Lk_w' + Dk_1] + k_1 2k_{-1}L\sqrt{k_w^*k_w}}{2([k_{-1}]^2L^2k_w^*)}$$

which gives the required square root dependence for low charging current density.

For large charging currents, consider the expressions

$$k_w^* \theta_w^2 + \left(k_1 + k_w' + k_w + k_{-1} C_{surf}\right)\theta_w - k_{-1} C_{surf} - k_w = 0$$

and

$$\frac{C_{surf}}{L} = \frac{k_1 \theta_w}{(k_{-1} L(1 - \theta_w) + D)}$$

as given above. For very large values of k_w and k_w', the first expression becomes

$$(k_w' + k_w)\theta_w - k_w = 0$$

so that

$$\theta_w = \frac{k_w}{(k_w' + k_w)}$$

and, substituting into the second expression,

$$\frac{C_{surf}}{L} = \frac{k_1 k_w}{\left(k_{-1} L k_w' + D(k_w' + k_w)\right)}$$

and if we write $k'_w = M\, k_w$ where we have used M = 1000, we get

$$\frac{C_{surf}}{L} = \frac{k_1}{\left(k_{-1} L M + D(M + 1)\right)}$$

as the asymptotic limit of the surface concentration for large values of *k*w and *kw'*.

This suggests that the relationship between the charging current and the surface concentration will be characterised by a square root proportionality for small charging currents and convergence to an asymptotic limit for large charging currents.

A set of numerical tests have been carried out to check this. The equation

$$D[k_{-1}]^2 L^2 A^3 + [([k_{-1}]^2 L^2 [k_w' + k_w^*] + D k_{-1} L[2k_1 + k_w' + k_w + 2k_w^*] + D^2 k_w^*)]A^2 + k_1\left[k_{-1} L[k_w' - k_w] + D[k_1 + k_w' + k_w]\right]A - k_w[k_1]^2 = 0$$

has been solved for the values given in the table above for various values of k_w, setting $k'_w = 1000\, k_w$ and this forms the basis of Figure 7 in the text.